Volume 84, July 2014

ISSN 0010-938X

ELSEVIER

CORROSION SCIENCE

The Journal on Environmental Degradation of Materials and its Control

Editor-in-Chief: G. T. BURSTEIN, University of Cambridge, U.K.

An Official Journal of the Institute of Corrosion

CONTENTS

Contents continued on outside back cover

http://www.elsevier.com/locate/corsci

Corrosion Science 84 (2014) 85–95

Contents lists available at ScienceDirect

Corrosion Science

journal homepage: www.elsevier.com/locate/corsci

An improved model for the corrosion of used nuclear fuel inside a failed waste container under permanent disposal conditions

Linda Wu [a], Zack Qin [a], David W. Shoesmith [a,b,*]

[a] Department of Chemistry, The University of Western Ontario, London, ON N6A 5B7, Canada
[b] Surface Science Western, The University of Western Ontario, London, ON N6G 0J3, Canada

ARTICLE INFO

Article history:
Received 1 January 2014
Accepted 7 March 2014
Available online 15 March 2014

Keywords:
A. Carbon steel
B. Modelling studies
C. Anodic dissolution
C. Interfaces

ABSTRACT

An improved model for nuclear fuel corrosion inside a failed waste container has been developed. The model considers the influence of the α-radiolysis products using a full radiolytic reaction set, and demonstrates that H_2O_2 is the dominant oxidant. Corrosion of the fuel is modelled considering both the direct oxidation of UO_2 by H_2O_2 and the galvanically-coupled oxidation by H_2O_2 reduction on noble metal (ε) particles. Corrosion has been found to be very sensitive to the corrosion products of steel container, Fe^{2+} and H_2. The surface coverage of ε-particles can significantly influence the dissolution rate.

1. Introduction

The safety assessment of deep geological disposal of used nuclear fuel requires a fundamental understanding of the processes controlling fuel corrosion and the release of radionuclides to the geosphere [1]. The development of source-term models to describe the processes involved in spent fuel dissolution has been the focus of considerable international effort [2–5]. The key process controlling the long-term release of radionuclides is corrosion of the UO_2 matrix [6]. In its reduced form (U^{IV}) the UO_2 matrix has an extremely low solubility in groundwater. However, the corrosion rate is very sensitive to the redox conditions since the solubility of the oxidized form (U^{VI}) is orders of magnitude higher [1,7]. Inside a failed waste container, the redox conditions at the fuel surface are controlled by both the oxidants/reductants produced by the radiolysis of the groundwater and the corrosion products of the steel container [8]. The radiolytic oxidants are expected to have a much larger influence on redox conditions than their reducing counterparts, at least during the early stages of disposal [9], and H_2O_2 has been shown to be the primary oxidant driving fuel corrosion [10,11]. However, the anaerobic corrosion of the steel container, sustained by H_2O reduction, will produce the potential redox scavengers, Fe^{2+} and H_2 [12].

A range of experimental studies has been conducted to determine how steel corrosion products would influence the fuel corrosion process. These studies have been recently reviewed [13] and are briefly discussed below. Ollila and co-workers [14–16] performed dissolution experiments on UO_2 doped with the α-emitter ^{233}U (to simulate the dose rates expected after 3000–10,000 years of disposal) in the presence of anaerobically corroding iron but found no evidence for irradiation-enhanced dissolution. These and similar experiments [3,14,15,17] suggested a significant reductive influence of the steel corrosion products and showed that both radiolytic oxidants and oxidized U^{VI} were reduced at the fuel surface. Corrosion studies using irradiated spent fuel segments [18–21] also showed that dissolved H_2 (in the concentration range 1–42 mmol L^{-1}) inhibited fuel dissolution. Cera et al. [22] observed in a long-term fuel leaching experiment that even radiolytically produced H_2 could inhibit fuel dissolution. The inhibiting effect of H_2 on UO_2 dissolution has been subsequently modelled by Eriksen and Jonsson [23] and Eriksen et al. [24].

In electrochemical experiments Broczkowski et al. observed a suppression of the corrosion potential by H_2 leading to a decrease in extent of surface oxidation on UO_2 specimens (SIMFUEL) doped to simulate the non-radioactive characteristics of spent fuel [25–27]. The extent of this effect was found to depend on the number density of noble metal particles in the SIMFUEL pellets and the concentration of dissolved H_2. It was proposed that fuel oxidation/dissolution was suppressed by H_2 oxidation on these particles galvanically coupled to the fission-product-doped UO_2 matrix. The kinetic parameters for reactions on UO_2 involving H_2 have

* Corresponding author at: Department of Chemistry, The University of Western Ontario, London, ON N6A 5B7, Canada. Tel.: +1 519 661 2111x86366; fax: +1 519 661 3022.
E-mail address: dwshoesm@uwo.ca (D.W. Shoesmith).

http://dx.doi.org/10.1016/j.corsci.2014.03.019
0010-938X/

been investigated [28–31] to facilitate the modelling of fuel dissolution rates.

The development of radiolytic models (in particular for α-radiolysis) for spent fuel corrosion has recently been reviewed [9]. Poinssot et al. [4] modelled fuel corrosion assuming that α-dose rate was uniform within a 45 μm thick water layer at the fuel surface, and that only half of the radiolytic oxidants reacted with the fuel, the remainder being consumed by other unidentified processes. A series of kinetic models, which included the influence of diffusive transport, were developed for both γ and α radiolytic processes by Christensen et al. [32] and Christensen [33], and a similar approach was adopted by Poulesquen and Jegou [34]. Since kinetic information for the reaction of radiolysis products with the fuel surface was unavailable, these models assumed that the heterogeneous reactions could be mimicked by an equivalent series of homogeneous reactions occurring within a thin layer of solution at the fuel surface. A mixed potential model based on electrochemical parameters for fuel corrosion was also developed [35,36]. This model included an attempt to model both the corrosion of the fuel and the steel vessel as well as a range of additional homogeneous redox reactions and adsorption/desorption/precipitation processes. The model also included reactions occurring on noble metal particles but not the influence of H_2. Jonsson et al. [37] developed a comprehensive model which integrated the available kinetic data and tried to account for the geometrical distribution of radiation dose rate and the effects of the oxidant scavengers Fe^{2+} and H_2, fuel burn up, and ground water chemistry. The maximum rate of spent fuel dissolution under Swedish repository conditions was calculated and it was concluded that a H_2 pressure of 0.1 bar (78 μmol L^{-1}) would be sufficient to completely suppress the corrosion of 100-year old LWR fuel even if the influence of Fe^{2+} was neglected. When the expected [Fe^{2+}] in a Swedish repository (~36 μmol L^{-1}) was included, its effect and that of the radiolytically produced H_2 alone were calculated to be sufficient to effectively inhibit fuel corrosion.

These studies have revealed many of the key features required in models for the radiolytic corrosion of spent fuel. The spatial distribution of radiolytic species is of particular importance for α-radiolysis since all the α-particle energy is deposited within a few tens of micrometers of the fuel/solution interface. Consequently, mass transport becomes important in coupling the homogeneous aqueous reactions and heterogeneous processes involved. This is especially important if the influence of container corrosion products, Fe^{2+} and H_2, on the redox conditions at the fuel surface are to be quantitatively modelled.

Previously [38], a preliminary model, involving a series of homogeneous and heterogeneous reactions, was developed to determine the influence of redox conditions on the radiolytic corrosion of spent fuel. The model also attempted to account rudimentarily for the separation of the two corroding interfaces at the fuel and the steel vessel surfaces. Consistent with the claims of Jonsson et al. [37], the model predicted that the corrosion of UO_2 could be suppressed by the steel corrosion products, Fe^{2+} and, in particular, H_2.

However, this model contained many approximations and limitations and has been improved in a number of ways: (i) A complete set of α-radiolytic reactions has been included. Previously, the α-radiolysis process was simplified with H_2O_2 considered the only radiolysis product. Inclusion of a full reaction set allows this simplification to be evaluated; (ii) A less arbitrary approach to account for the decomposition of radiolytically-produced H_2O_2 has been adopted, since this process appears to be the major route for H_2O_2 consumption on a UO_2 surface [10,39]; (iii) An attempt to incorporate the influence of fuel burnup is included, since burnup will not only influence the dose rate but also affect the surface reactivity of the fuel [40]; (iv) Instead of treating the oxidative dissolution (corrosion) of UO_2 as a general surface reaction, an attempt is made to take into account anodic dissolution supported by H_2O_2 reduction on both the UO_2 and noble metal particle surfaces, the latter being a product of the in-reactor fission process; and (v) the reactions between H_2 and H_2O_2 and between H_2 and UO_2^{2+} catalyzed on noble metal particles have been added. As in the previous model it is assumed that the groundwater contains sufficient carbonate/bicarbonate and any formation of corrosion product deposits is omitted, thus making the predicted dissolution rate conservative.

Presently, as is the case with other models, our model is 1-dimensional and considers only the corrosion of a planar fuel surface. However, this is a precursor for the eventual development of 2-D and 3-D models involving customized geometry to account for the fractured nature of the spent fuel and the complex fuel bundle geometry. Within such structures the local accumulation of radiolysis species is likely to occur and externally produced Fe^{2+} and H_2 may have limited access to reactive locations within fractures, porous grain boundaries and fuel bundles. Such geometric effects are expected to have a significant influence on the overall ability of container corrosion products to influence fuel corrosion and radionuclide release.

2. Model description

During in-reactor irradiation, the UO_2 fuel pellet undergoes a number of compositional changes involving the formation of rare earth (RE^{III}) elements and noble metal (ε) particles [8,38]. From a corrosion perspective, the fuel can be considered as a conductive (RE^{III}-doped) and chemically reactive matrix containing ε-particles which could act as either cathodes or anodes depending on the prevailing solution redox conditions. The reaction set used to describe the fuel corrosion process is modified compared to that used previously, as numbered and illustrated in Fig. 1. The current model includes: (1) a complete reaction set for the α-radiolysis of water including the generation of, and the interactions between, the radiolysis products; (2) the oxidative dissolution (corrosion) of UO_2 supported by H_2O_2 reduction on both the UO_2 surface (reaction 2a) and noble metal particles (reaction 2b); (3) the reduction of oxidized surface species (U^V/U^{VI}) by H_2 oxidation on noble metal particles (reaction 3a) and of dissolved UO_2^{2+} either by reaction with H_2 in solution (reaction 3b) or with H_2 catalyzed on the fuel surface (reaction 3c); (4) the reaction of H_2O_2 with H_2 catalyzed by noble metal particles; (5) the scavenging of H_2O_2 in homogeneous solution by reaction with Fe^{2+}; and (6) the decomposition of H_2O_2 to O_2 and H_2O (not shown in Fig. 1). In the model the rates of these processes are described by a series of one dimensional diffusion–reaction equations as described previously [38] .

2.1. Water radiolysis

Since it is reasonable to assume containment preventing contact of the fuel with groundwater will be maintained over the period when γ/β radiation fields are significant (a few hundred years), only α-radiolysis is considered as a source of oxidants [6]. The penetration depth of α-particles emitted by spent fuel into water is very short and a high concentration of radiolysis species is expected at the fuel/water interface. Due to the fractured nature of spent fuel, the accumulation of aqueous radiolysis species may occur locally within cracks, fission gas tunnels and porous grain boundaries. These features are not considered in this model which focuses on the general corrosion of a uniform fuel surface.

A range of studies have calculated the dose rate profiles of α-radiation for different types of fuels using different approaches [41–44]. The α dose rate in water in contact with a spent fuel

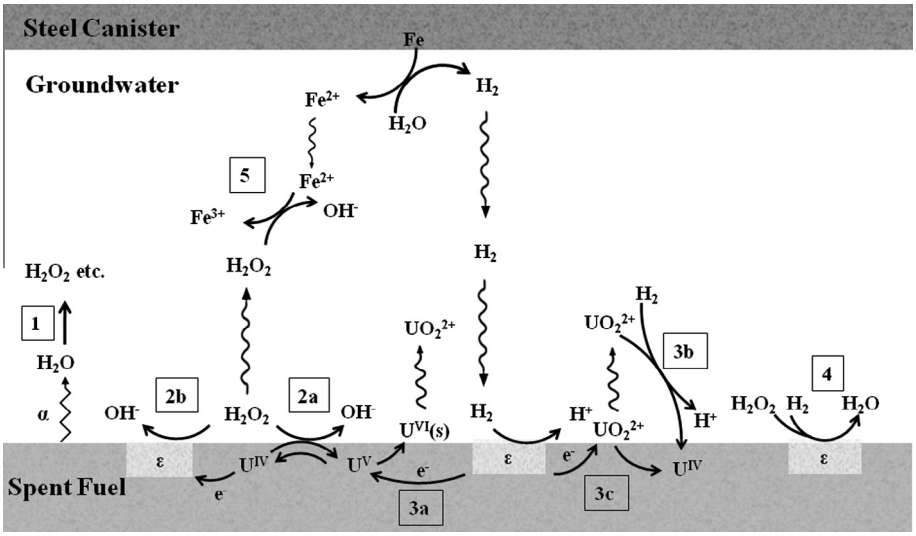

Fig. 1. Reactions included in the model for the α-radiolytic corrosion of spent nuclear fuel. This diagram is an improved version from previous work [38].

bundle is determined by the source activity (which varies with different types of fuel, burnup and fuel age), the radiation energy and the distance from the source [45]. A typical energy of the alpha particles from fuel decay is 5 MeV, corresponding to a path length of ~40 μm in water [34]. However, before reaching the fuel surface the alpha particles are attenuated by passage through the UO_2 matrix, and escape into the water with a reduced energy between 0 and 5 MeV. This was accounted for in the previous calculations [42,43] by integrating all contributions as a function of the distance travelled within the fuel. The geometrical distribution of α dose rate in a water layer of ~40 μm has been found to follow an exponential decay with distance from the fuel surface [42]. According to the Bragg curve, which describes the extent of ionization along the radiation pathway [34], the radiolysis species are non-uniformly distributed along this pathway. Garisto et al. [41] adopted a different methodology [44,46] using the thermal power of the fuel and the ratio between the specific stopping power values in water and in UO_2. This lead to an average energy of 2.5 MeV for the α particles emitted from the fuel surface, i.e., one half of the unattenuated energy assuming a uniform distribution of radionuclides and isotropic decay [41]. Based on this assumption, the authors calculated the range of α-radiation in water to be 13 μm, corresponding to an energy of 2.5 MeV, and an average dose rate within this range. These different methodologies have been demonstrated to be in good agreement [43]. In our previous model [38] it was shown that, from the radiolytic corrosion perspective, it was reasonable to consider the α dose rate as uniformly distributed within this range. In this study, we adopted the values of α dose rate and range calculated by Garisto et al. [41] for the radionuclide inventories of CANDU used fuel.

The one-dimensional arrangement used to describe the fuel/groundwater interface remains the same as that used previously [38]. A thin layer of solution at the fuel/water interface with a thickness of 13 μm is designated the radiation zone. No radiolysis species are produced beyond this zone. The diffusion layer is the distance over which species can diffuse to, or from, the fuel surface and beyond which uniform concentrations are presumed to prevail. The bulk concentrations of H_2 and Fe^{2+} are assumed to depend on the corrosion behaviour of the steel vessel, and the concentrations of all radiolytic species and fuel corrosion products are assumed to be zero in the bulk solution. The thickness of the diffusion zone represents an arbitrary boundary beyond which the concentration of all species, irrespective of where they are produced, is assumed to become uniform. Clearly, this assumption is sensitive to the geometrical conditions within the failed container as discussed previously [38]. For a one-dimensional model, our previous calculations [38] showed an insignificant dependence of the fuel corrosion rate on the chosen value of this thickness.

The interaction of α-radiation with water yields a series of decomposition products (H_2, H_2O_2, $H^{\cdot}$, $OH^{\cdot}$, $HO_2^{\cdot}$, e_{aq}^-, H^+ and OH^-) [45,47], among which the molecular species are dominant. The radical species have concentrations orders of magnitude lower than those of the stable molecular products as a consequence of their high reactivity and consequently short lifetimes. Since H_2O_2 has been demonstrated to be the primary oxidant in the radiolytic corrosion of the fuel [2,11], it was the only radiolysis product included in the previous model.

The primary yields of radiolysis species are expressed by g-values (the number of moles formed per joule of radiation energy absorbed), as listed in Table 1. The rate of radiolytic production for species i is calculated using the expression

$$R_i = D_R \cdot g_i \cdot \rho_{H_2O} \quad (0 \leqslant x \leqslant b) \tag{1}$$

where D_R is the dose rate representing the rate of energy deposited per unit of mass, g_i is the g-value of species i, and ρ_{H_2O} is the density of water. Both oxidizing molecular and radical species (e.g. H_2O_2, O_2, $OH^{\cdot}$) and reducing species (e.g. H_2, $H^{\cdot}$, e_{aq}^-) are formed. After formation, these radiolytic species undergo diffusion and a series of chemical reactions (Table 2). All these species are used when calculating the consequences of aqueous radiolysis. However, in the simultaneous corrosion reactions only the molecular species

Table 1
The primary yields (g-values) of α radiolysis species used in model calculations.

Water decomposition species	g-value (μmol/J) [73]
H_2	0.1248
H_2O_2	0.104
e_{aq}^-	0.0156
$H^{\cdot}$	0.0104
$OH^{\cdot}$	0.0364
$HO_2^{\cdot}$	0.0104
H^+	0.01872
OH^-	0.00312

Table 2
Full radiolysis reaction set and rate constants/equilibrium constants used in model calculations [62,80].

Reaction	Rate constant at 25 °C (L mol^{-1} s^{-1} or s^{-1})[a]
$H_2O \xrightarrow{\alpha} H_2, H_2O_2, e^-_{aq}, H^\cdot, OH^\cdot, HO_2^\cdot, H^+OH^-$	*g*-values in Table 1
$e^-_{aq} + e^-_{aq}(+2H_2O) \rightarrow H_2 + 2OH^-$	7.26×10^9
$e^-_{aq} + H^\cdot(+H_2O) \rightarrow H_2 + OH^-$	2.76×10^{10}
$e^-_{aq} + OH^\cdot \rightarrow OH^-$	3.5×10^{10}
$e^-_{aq} + H_2O_2 \rightarrow OH^\cdot + OH^-$	1.4×10^{10}
$e^-_{aq} + O_2 \rightarrow O_2^-$	2.3×10^{10}
$e^-_{aq} + HO_2^\cdot \rightarrow HO_2^-$	1.3×10^{10}
$e^-_{aq} + O_2^-(+H_2O) \rightarrow H_2O_2 + 2OH^-$	1.3×10^{10}
$H^\cdot + H^\cdot \rightarrow H_2$	5.13×10^9
$H^\cdot + OH^\cdot \rightarrow H_2O$	1.1×10^{10}
$H^\cdot + H_2O_2 \rightarrow OH^\cdot + H_2O$	3.6×10^7
$H^\cdot + O_2 \rightarrow HO_2^\cdot$	1.3×10^{10}
$H^\cdot + HO_2^\cdot \rightarrow H_2O_2$	1.13×10^{10}
$H^\cdot + O_2^- \rightarrow HO_2^-$	1.13×10^{10}
$H^\cdot + H_2O \rightarrow H_2 + OH^\cdot$	4.58×10^{-5}
$OH^\cdot + OH^\cdot \rightarrow H_2O_2$	4.8×10^9
$OH^\cdot + H_2O_2 \rightarrow HO_2^\cdot + H_2O$	2.9×10^7
$OH^\cdot + H_2 \rightarrow H^\cdot + H_2O$	3.9×10^7
$OH^\cdot + HO_2^\cdot \rightarrow O_2 + H_2O$	8.8×10^9
$OH^\cdot + O_2^- \rightarrow O_2 + OH^-$	1.1×10^{10}
$OH^\cdot + HO_2^- \rightarrow O_2^- + H_2O$	8.1×10^9
$H_2O_2 \rightarrow 2OH^\cdot$	8.29×10^{-8}
$HO_2^\cdot + HO_2^\cdot \rightarrow H_2O_2 + O_2$	8.4×10^5
$O^- + HO_2^- \rightarrow O_2^- + OH^-$	7.8×10^8
$O^- + O_2 \rightarrow O_3^-$	3.7×10^9
$O^- + H_2 \rightarrow H^\cdot + OH^-$	1.3×10^8
$O_2^- + HO_2^\cdot(+H_2O) \rightarrow H_2O_2 + O_2 + OH^-$	1×10^8
$O_2^- + O_2^-(+2H_2O) \rightarrow H_2O_2 + O_2 + 2OH^-$	3×10^{-1}
$O_3^- \rightarrow O^- + O_2$	2.6×10^3
$O_3^- + H_2O_2 \rightarrow O_2 + O_2^-(+H_2O)$	1.6×10^6
$O_3^- + H_2 \rightarrow O_2 + H^\cdot + OH^-$	2.5×10^5
$O_3^- + HO_2^- \rightarrow O_2 + O_2^- + OH^-$	8.9×10^5
Equilibrium reaction	**K_{eq} at 25 °C (mol L^{-1} or no unit)[b]**
$H_2O \rightleftharpoons H^+ + OH^-$	1.80×10^{-16}[c]
$H_2O_2 \rightleftharpoons H^+ + HO_2^-$	1.88×10^{-12}
$H_2O_2 + OH^- \rightleftharpoons HO_2^- + H_2O$	1.04×10^4
$OH^\cdot \rightleftharpoons H^+ + O^-$	1.88×10^{-12}
$OH^\cdot + OH^- \rightleftharpoons O^- + H_2O$	1.04×10^4
$HO_2^\cdot \rightleftharpoons H^+ + O_2^-$	1.54×10^{-5}
$HO_2^\cdot + OH^- \rightleftharpoons O_2^- + H_2O$	8.56×10^{10}
$H^\cdot \rightleftharpoons H^+ + e^-_{aq}$	2.78×10^{-10}
$H^\cdot + OH^- \rightleftharpoons e^-_{aq} + H_2O$	1.55×10^6

[a] Unit for reaction rate constant: L mol^{-1} s^{-1} for second-order reactions; and s^{-1} for first-order reactions. If water is provided in brackets, it is not counted when determining the reaction order.

[b] Unit for equilibrium constant: mol L^{-1} for the reaction type A ↔ C + D; and no unit for A + B ↔ C + D.

[c] The following definition of the equilibrium constant for the dissociation of water is used: $K_{eq}(H_2O) = [H^+][OH^-]/[H_2O]$, where $[H_2O]$ is 55.417 mol L^{-1} at 25 °C [62]. Similarly, in the other equilibrium reactions involving H_2O, this value of $[H_2O]$ is also used.

(H_2O_2, O_2 and H_2) are considered, since the radical species, although reactive with the UO_2 surface, have low concentrations as a consequence of their short lifetimes. Calculations for various radicals yield concentrations which are 2–5 orders of magnitude lower than those of the stable molecular products (Section 3.1 below). This approximation is consistent with other studies which also show the radical species produced by α-radiolysis have an insignificant impact on UO_2 corrosion compared to H_2O_2 [10,11].

The higher *g*-values for molecular compared to radical species, Table 1, are attributable to the fact α-radiation is a high linear energy transfer (LET) radiation which produces a high density of spurs leading to extensive recombination of radicals to produce stable molecular/ionic species. The relatively low g-values of radical species also partially account for their low concentrations. The molecular reductant, H_2, is inert compared to the oxidant, H_2O_2, and has a higher diffusivity and, hence, a relatively smaller impact at the UO_2 surface. Thus, the redox conditions at the fuel surface appear to be dominantly oxidizing, at least during the early stages of disposal when the fuel matrix is in its reduced form (U^{IV}) [9].

2.2. UO_2 oxidation by H_2O_2

Both the UO_2 surface and ε-particles can support the cathodic reduction of H_2O_2 to drive the anodic dissolution of UO_2 [48,49]. Since the number density of ε-particles will vary with fuel burnup, the adoption of a single rate constant for the uniform cathodic reactivity of the fuel surface will not be able to account for the influence of an increasing number of ε-particles as burnup increases. The current model is improved by including two distinct reactions:

(i) the direct reaction of UO_2 with H_2O_2, reaction (2a) in Fig. 1,

$$UO_2 + H_2O_2 \xrightarrow{k_{2a}} UO_2^{2+} + 2OH^- \quad (2)$$

and; (ii) the catalyzed oxidation of UO_2, reaction (2b) in Fig. 1, involving the galvanic coupling of H_2O_2 reduction on ε-particles to UO_2 oxidation:

$$UO_2 + H_2O_2 \xrightarrow[\varepsilon]{k_{2b}} UO_2^{2+} + 2OH^- \quad (3)$$

In the previous model [38] UO_2 oxidation/dissolution was assumed to proceed as a pseudo first order reaction, with the available UO_2 surface in excess compared to the oxidants, with an overall rate constant, k_2,

$$UO_2 + H_2O_2 \xrightarrow{k_2} UO_2^{2+} + 2OH^- \quad (4)$$

$$R_2 = k_2 \cdot [H_2O_2] \quad (x = 0) \quad (5)$$

In the absence of a measured rate constant for this reaction on actual spent fuel, a value of 7.33×10^{-5} m s^{-1} was adopted as an upper limit in the simulations of Nielsen et al. [50]. This limiting value was arbitrarily adopted in our previous model to avoid underestimating the experimentally demonstrated catalysis of corrosion by H_2O_2 reduction on ε-particles galvanically coupled to the UO_2 matrix. Some experimental evidence to support the adoption of this value was presented [25,27,38]. The use of this rate constant was considered conservative.

As stated above, the improved model separates this reaction into distinct reactions on UO_2 and ε-particles, reactions (2a) and (2b) in Fig. 1. Reaction (2a) is expressed as a first-order reaction with respect to $[H_2O_2]$

$$R_{2a} = k_{2a} \cdot [H_2O_2] \quad (x = 0) \quad (6)$$

The rate constant for the UO_2 oxidative dissolution adopted in the model, $k_{2a} = 1.0 \times 10^{-8}$ m s^{-1}, was measured on a pure UO_2 pellet fabricated by Westinghouse [39]. Recently, Nilsson et al. [51] and Pehrman et al. [39] have reported that only a small portion of the H_2O_2 consumed on a UO_2 surface resulted in UO_2 oxidation (Section 2.6 below).

The catalytic reaction (2b) is also taken to be first-order with respect to H_2O_2 taking into account the surface fraction of ε-particles,

$$R_{2b} = k_{2b} \cdot s_\varepsilon \cdot [H_2O_2] \quad (x = 0) \quad (7)$$

where s_ε is the fraction of fuel atoms that underwent fission to yield noble metal (ε) particles, e.g. 1.0 at.%. The experimental value for this catalytic rate constant k_{2b} is 6.92×10^{-6} m s^{-1} [52]. The total reaction rate is the sum of R_{2a} and R_{2b}:

$$R_{2\_total} = R_{2a} + R_{2b} = k_{2b} \cdot [H_2O_2] + k_{2b} \cdot s_\varepsilon \cdot [H_2O_2] \quad (x = 0) \quad (8)$$

As in the first version of the model, these reactions are taken to proceed unimpeded by the accumulation of corrosion product deposits, a situation that would prevail in the presence of a sufficient groundwater concentration of HCO_3^-/CO_3^{2-}.

The influence of the additional molecular oxidant, O_2, was also considered. This oxidant can be formed directly by α-radiolysis or by H_2O_2 decomposition. However, sensitivity calculations show its inclusion has no significant effect on the fuel corrosion rate. This is not unexpected since the steady-state concentration of radiolytically-produced O_2 appears to be two orders of magnitude lower than that of H_2O_2 (see Section 3.1), and the rate constant for the reaction between O_2 and UO_2 is 1/200th that of the reaction between H_2O_2 and UO_2 [2]. A similar conclusion was reached based on α-radiolysis simulations by Ekeroth et al. [11] and on experiments on UO_2 powder/pellets by Lousada et al. [10]. By contrast, on SIMFUEL the reaction with O_2 accounted for ~30% of the UO_2 corrosion since a significant amount of H_2O_2 was consumed by decomposition [10]. The consequences of H_2O_2 decomposition are discussed in Section 2.6.

2.3. U^V/U^{VI} reduction by H_2

Hydrogen has been shown to suppress UO_2 corrosion on a range of UO_2 materials ranging from spent fuel itself to α-doped UO_2 and SIMFUELs [12,52–54]. The main source of H_2 within a failed container is the anaerobic corrosion of the steel vessel, and dissolved H_2 concentrations as high as 0.038 mol L^{-1} are anticipated in sealed repositories [53]. There appear to be three possible pathways for reaction between U^V/U^{VI} and H_2 as numbered in Fig. 1.

Reaction (3a): A key mechanism for the inhibition of corrosion by H_2 has been demonstrated to be the galvanic coupling of H_2 oxidation on ε-particles to UO_{2+x} reduction on the fuel surface [12,25–27], with the oxidation/dissolution process appearing to be reversed at the U^V stage [27]. As described in the previous model [38], the overall reaction can be expressed as involving a U^{VI} surface intermediate which can act as a precursor to dissolution, reaction (3a) in Fig. 1,

$$U^{VI}(s) + H_2 \xrightarrow[\varepsilon]{k_{3a}} U^{IV} + 2H^+ \quad (9)$$

with a reaction rate R_{3a}, derived by Trummer et al. [29], to be

$$R_{3a} = k_{3a} \cdot s_\varepsilon \cdot [H_2] \quad (x = 0) \quad (10)$$

The measured rate constant (k_{3a}) was found to vary slightly with the amount of Pd present (added to simulate the presence of ε-particles) with values close to the diffusion controlled limit [29].

Reaction (3b): The reduction of dissolved UO_2^{2+} in the bulk of solution via a homogeneous reaction with H_2 [28], reaction (3b) in Fig. 1,

$$UO_2^{2+}(aq) + H_2 \xrightarrow{k_{3b}} UO_2 + 2H^+ \quad (11)$$

with the reaction rate determined by a second-order rate constant, k_{3b},

$$R_{3b} = k_{3b} \cdot [H_2] \cdot [UO_2^{2+}] \quad (0 \leqslant x \leqslant L) \quad (12)$$

This reaction is not expected to influence the release of radionuclides but only to lower the bulk concentration of UO_2^{2+}, assuming that the radionuclides (e.g. ^{99}Tc, ^{129}I, ^{79}Se, ^{135}Cs [7]) trapped within the fuel matrix are released irreversibly on UO_2 dissolution. The rate of this reaction is expected to be very low considering the low concentrations and the small rate constant, k_{3b} in Table 3.

Reaction (3c): Nilsson et al. [31] have claimed that the reaction (11) can also be catalyzed on the surface of ε-particles leading to a significant increase in its rate, based on experiments using Pd in aqueous UO_2^{2+} solution with a H_2 atmosphere. This surface catalytic reaction,

$$UO_2^{2+}(aq) + H_2 \xrightarrow[\varepsilon]{k_{3c}} UO_2 + 2H^+ \quad (13)$$

is shown as reaction (3c) in Fig. 1 and has a reaction rate given by

$$R_{3c} = k_{3c} \cdot s_\varepsilon \cdot [UO_2^{2+}] \quad (x = 0) \quad (14)$$

Reaction (3c) is also not expected to change the release rate of radionuclides but only to lower the surface $[UO_2^{2+}]$. Sensitivity tests performed for this reaction show it has a marginal overall effect due to the low surface concentration of UO_2^{2+}. However, this reaction could have a larger impact in the presence of a high $[UO_2^{2+}]$ which could be the case when the behaviour in fuel fractures is considered. This effect is under investigation in the development of a 2-dimensional model.

2.4. Reaction between H_2O_2 and H_2

Catalysis of the reaction between H_2 and H_2O_2 has been demonstrated experimentally on Pd particles [30],

Table 3
Default values of simulation parameters.

Parameter	Symbol	Value	Unit
Diffusion layer thickness [38]	L	10^{-3}	m
Radiation zone thickness [41]	b	1.3×10^{-5}	m
Alpha radiation dose rate[a] [41]	D_R	9.03×10^5	Gy a^{-1}
ε-particle coverage [74]	s_ε	0.01	–
UO_2 pellet oxidation rate const. in H_2O_2 [39]	k_{2a}	1.0×10^{-8}	m s^{-1}
H_2O_2/UO_2 surf. reaction rate const. on ε [52]	k_{2b}	6.92×10^{-6}	m s^{-1}
H_2/U^{VI} surf. reaction rate const. on ε [29]	k_{3a}	4×10^{-7}	m s^{-1}
H_2/UO_2^{2+} bulk reaction rate const. [28]	k_{3b}	3.6×10^{-9}	L mol^{-1} s^{-1}
H_2/UO_2^{2+} surf. reaction rate const. on ε [31]	k_{3c}	1.5×10^{-5}	m s^{-1}
H_2/H_2O_2 surf. reaction rate const. on ε [30]	k_4	2.2×10^{-5}	m s^{-1}
Fe^{2+} bulk reaction rate const. [55]	k_5	1×10^6	L mol^{-1} s^{-1}
H_2O_2 homogeneous decomp. rate const. [62]	k_{6a}	8.29×10^{-8}	s^{-1}
H_2O_2 surface-catalyzed decomp. rate const.[b] [39]	k_{6b}	6.14×10^{-8}	m s^{-1}

[a] The unit Gy a^{-1} stands for the absorbed dose per annum. One gray (Gy) is the absorption of one joule of energy, in the form of ionizing radiation, per kilogram of matter. The value used in this model, 9.03×10^5 Gy a^{-1}, is corresponding to CANDU fuel with a burnup of 220 MW h kg U^{-1} at 1000 years after discharge from reactor [41].

[b] The rate constant of the surface catalyzed decomposition was calculated using the rate constant of the UO_2 oxidation and the dissolution yield (14%) measured on the Westinghouse UO_2 pellet [39]. The dissolution yield was based on the ratio between dissolved $[U^{VI}]$ and consumed $[H_2O_2]$ and the difference (86%) was attributed to catalytic decomposition of H_2O_2.

$$H_2O_2 + H_2 \xrightarrow[\varepsilon]{k_4} 2H_2O \quad (15)$$

This reaction was found to be first order with respect to $[H_2O_2]$, but independent of H_2 pressure in the pressure range 1–40 bar [30]. Thus, the overall reaction rate can be expressed by

$$R_4 = k_4 \cdot s_\varepsilon \cdot [H_2O_2] \quad (0 \leqslant x \leqslant L) \quad (16)$$

where the reaction rate constant, k_4, was measured to be 2.2×10^{-5} m s^{-1}. This recombination reaction can reduce the surface concentrations of both H_2 and H_2O_2. A sensitivity test has been performed and the surface $[H_2O_2]$ is shown to decrease marginally (7%) in the presence of this reaction compared to that in its absence.

2.5. Fenton reaction

Besides H_2, the anaerobic corrosion of the steel vessel can produce Fe^{2+} ions that can react with H_2O_2 in the homogeneous Fenton reaction.

$$Fe^{2+} + H_2O_2 \rightarrow Fe^{3+} + OH^- + OH^\cdot \quad (17)$$

$$Fe^{2+} + OH^\cdot \rightarrow Fe^{3+} + OH^- \quad (18)$$

As in the previous model [38], the $OH^\cdot$ radicals produced as intermediates in reaction (17) have been assumed to all be consumed in reaction (18). The overall reaction can be expressed as

$$2Fe^{2+} + H_2O_2 \rightarrow 2Fe^{3+} + 2OH^- \quad (19)$$

and is a second order reaction [55] with a rate given by

$$R_5(Fe^{2+}) = 2R_5(H_2O_2) = -k_5[Fe^{2+}][H_2O_2] \quad (0 \leqslant x \leqslant L) \quad (20)$$

The rate of this reaction has been shown to be very sensitive to pH, temperature and salinity. Considering the long-term disposal conditions (e.g. pH 8–10, 25 °C, groundwater) [56–58], the value of k_5 has been assumed to be 1×10^6 L mol^{-1} s^{-1} in this model [55]. Within the anticipated pH range, the solubility of Fe^{2+} is in the region of 10^{-6} to 10^{-4} mol L^{-1}, although the actual $[Fe^{2+}]$ could vary depending on the corrosion behaviour of the steel vessel [59].

2.6. H_2O_2 decomposition

The decomposition of H_2O_2 can form oxygen and water by the overall reaction,

$$2H_2O_2 \rightarrow O_2 + 2H_2O \quad (21)$$

It has been well established that this reaction follows first order kinetics, with an activation energy measured to be 42–65 kJ/mol over a wide range of temperatures [60–62]. However, the decomposition mechanism is not fully understood, the key question being whether or not the initiating step is H_2O_2 dissociation to form two hydroxyl radicals,

$$H_2O_2 \rightarrow 2OH^\cdot \quad (22)$$

or the formation of some other intermediate that could occur on a metal/metal-oxide surface. Wren et al. [63] proposed a mechanism of H_2O_2 decomposition catalyzed by U^{IV}/U^V surface species, but did not study the kinetics. Lousada and co-workers performed a series of experimental and density functional theory investigations [10,64,65] to show the formation of $OH^\cdot$ will be a primary product during H_2O_2 decomposition on UO_2 and other transition metal oxide surfaces. Recently, Nilsson et al. [51] and Pehrman et al. [39] studied the kinetics of the catalytic decomposition of H_2O_2 on different UO_2 pellets (pure UO_2, doped UO_2, and SIMFUEL) by monitoring the $OH^\cdot$ production and concluded that the decomposition rate was virtually independent of matrix doping. They also measured the dissolution yield based on the ratio between the concentrations of dissolved U^{VI} and consumed H_2O_2 and attributed the difference between them to the catalytic decomposition of H_2O_2. These results indicate that the surface-catalyzed decomposition of H_2O_2 is the major pathway for its consumption as opposed to H_2O_2-promoted UO_2 dissolution. Interestingly, the dissolution yield for the pure UO_2 pellet (14%) was much higher than that for the SIMFUEL pellet (0.2%). Recent electrochemical results suggest this is most likely due to stabilization of the UO_2 lattice due to fission product doping [66].

The H_2O_2 decomposition rate is sensitive to many features including temperature, pH and the presence of solid/soluble catalysts [67–71]. The uncertainty about disposal conditions makes the choice of a rate constant arbitrary. Since H_2O_2 is the primary oxidant involved in fuel corrosion, and its decomposition by various reaction pathways would inevitably lead to a decrease in corrosion rate, a worst-scenario approach (estimating the highest corrosion rate) has been adopted when modelling the H_2O_2 decomposition. Therefore, $Fe^{II/III}$ catalyzed decomposition is not included in the model.

This model includes both the uncatalyzed homogeneous decomposition in solution and the catalyzed decomposition on the UO_2 surface. For the homogeneous decomposition, we adopted reaction (22) using a rate constant of 8.29×10^{-8} s^{-1} (k_{6a} in Table 3) [62]. For the surface-catalyzed decomposition, the rate constant, k_{6b}, was adopted from measurements on UO_2 pellets [39] using the relationship that 14% of H_2O_2 consumption on the UO_2 surface (not including ε-particles) went to fuel dissolution and the remainder, 86%, to H_2O_2 decomposition. The reason for the low dissolution yield on SIMFUEL [51], as discussed above, was not clear. The possibility of decomposition catalyzed by ε-particles is under investigation and preliminary results suggest this pathway is insignificant under corrosion conditions. Based on this study, decomposition of H_2O_2 catalyzed by ε-particles was not included in this model.

3. Results and discussion

The mathematical model outlined above was numerically simulated using COMSOL Multiphysics based on the finite element method. The model was developed using the chemical engineering module and the diluted species transportation module of COMSOL Multiphysics (version 4.3.0.151, COMSOL Inc.). Calculations were performed to evaluate the effects of a full α-radiolysis reaction set, $[Fe^{2+}]_{bulk}$, $[H_2]_{bulk}$, the surface coverage by ε-particles and the age of the fuel. The default values of the simulation parameters are listed in Table 3. The parameters were maintained at the default values for all calculations unless otherwise stated.

3.1. The effect of including a full α-radiolysis reaction set

The calculated results for the steady-state concentration profiles of radiolysis species and corrosion products are plotted in Fig. 2. The molecular species H_2O_2 and H_2 are predicted to have the highest concentrations, ~10 nmol L^{-1} near the fuel surface and approaching zero along the diffusion pathway. The molecular product, O_2, has a lower concentration of around 0.3 nmol L^{-1} including the contribution from H_2O_2 decomposition. Concentrations of the other radiolysis species ($OH^\cdot$, $H^\cdot$, O_2^-, HO_2^-, e_{aq}^-) are 2–5 orders of magnitude lower than $[H_2O_2]$. Beyond the radiation zone ($x > 1.3 \times 10^{-2}$ mm), the $[OH^\cdot]$, $[H^\cdot]$ and especially $[e_{aq}^-]$ drop rapidly due to their high reactivity. The concentration of the corrosion product, UO_2^{2+}, exhibits a straight line if plotted linearly against distance, with a maximum of ~1 nmol L^{-1} at the fuel surface and decreasing to zero at the diffusion zone boundary ($x = L$). The slope of the line indicates a steady-state flux of UO_2^{2+} to the bulk solution, i.e., a constant UO_2 corrosion rate.

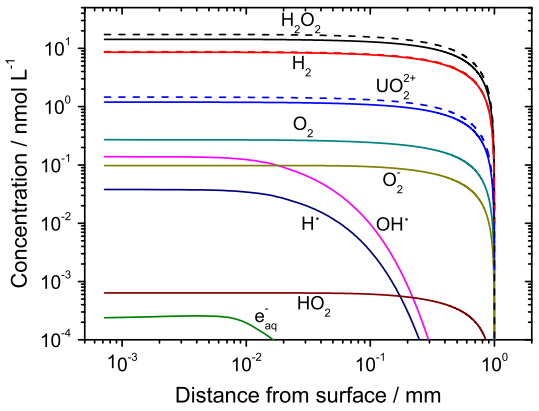

Fig. 2. The steady-state concentration profiles of α radiolysis species and dissolved UO_2^{2+} as a function of distance from the fuel surface; $[H_2]_{bulk} = [Fe^{2+}]_{bulk} = 0$. The solid lines are the model predictions using the full radiolysis reaction set, and the dashed lines are the estimated concentrations based on the radiolytic production of only H_2O_2 and H_2.

Fig. 2 also includes the concentration-distance profile (shown as dashed lines) calculated using only the radiolysis production of the molecular species (H_2O_2, H_2). This simplified calculation uses a slightly larger g-value for H_2O_2. In Table 1, the *g*-values used in the radiolysis reaction set are 0.104 μmol J^{-1} for H_2O_2 and 0.1248 μmol J^{-1} for H_2. The simplified calculation makes a conservative assumption that all the other radicals are recombined to produce H_2O_2 ($2OH^{\cdot} \rightarrow H_2O_2$, $H^{\cdot} + HO_2^{\cdot} \rightarrow H_2O_2$) and the overall g-value of H_2O_2 is assumed to be 0.1248 μmol J^{-1} considering the mass balance during the radiolytic decomposition ($2H_2O \rightarrow H_2 + H_2O_2$). The comparison in Fig. 2 shows that the simplified calculation overestimates the $[H_2O_2]$ by ~21% and $[H_2]$ by ~3%, leading to a faster corrosion rate which is indicated by an increase of ~20% in the $[UO_2^{2+}]$ profile. Although the plots in Fig. 2 assume no interference from the steel corrosion products, a similar trend is observed in the presence of external H_2 and Fe^{2+}, Fig. 3. The lower $[H_2O_2]$ calculated when using the full radiolysis reaction set is likely due to H_2O_2 consumption by reactions with reducing species such as $H^{\cdot}$, e^-_{aq}, and H_2.

This simulation result is consistent with published literature. Corbel et al. [72] investigated the effect of α-radiolysis on UO_2 corrosion using a synchrotron alpha beam (E_α = 5–8 MeV). A linear dependence of the radiolytic $[H_2O_2]$ on absorbed radiation energy was observed, with a slope similar to the radiolytic yields of H_2O_2. Pastina et al. [73] also measured H_2O_2 production in α-irradiated water (E_α = 5 MeV) saturated with Ar and found the observed production rate was slightly lower than the predicted rate

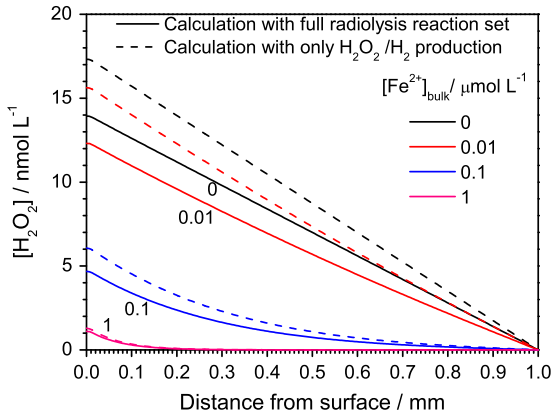

Fig. 3. Steady-state $[H_2O_2]$ profiles calculated for various bulk $[Fe^{2+}]$; $[H_2]_{bulk}$ = 0.01 μmol L^{-1}. The solid lines are the model predictions using the full radiolysis reaction set, and the dashed lines are the estimated concentrations based on only radiolytic production of H_2O_2 and H_2.

based on a model which used only the radiolytic yield of H_2O_2. It can be concluded that using only the radiolytic production of H_2O_2 and H_2 to simulate α-radiolysis is an acceptable estimation and has the advantage of a much shorter calculation time. All the modelling calculations in this paper, other than those presented in Figs. 2 and 3, still use the full radiolysis reaction set to account for the radiolysis effect. It is expected that the above simplification can be used for the more complicated calculations involved with 2-D and 3-D models.

3.2. Suppression of UO_2 corrosion by Fe^{2+}

Fig. 3 shows the influence of Fe^{2+} on the $[H_2O_2]$ profile in the $[Fe^{2+}]_{bulk}$ range of 0.01–1 μmol L^{-1}. In the absence of Fe^{2+}, H_2O_2, at locations away from the UO_2 surface, is consumed only by its slow decomposition thus the maximum concentration is achieved. Beyond the radiation zone, the $[H_2O_2]$ decreases linearly along the diffusion pathway and reaches zero at the diffusion boundary indicating a constant H_2O_2 flux outwards to the bulk solution. For $[Fe^{2+}]_{bulk} \leqslant 0.01$ μmol L^{-1}, the consumption of $[H_2O_2]$ by the Fenton reaction is minor, the almost linear $[H_2O_2]$ profile approaching that calculated in the absence of Fe^{2+}. As the $[Fe^{2+}]_{bulk}$ increases to 0.1 μmol L^{-1}, the surface $[H_2O_2]$ rapidly decreases to one third of the maximum value. When approaching the solubility limit ($[Fe^{2+}]_{bulk}$ = 1 μmol L^{-1}), the surface $[H_2O_2]$ is suppressed to only 10% of its maximum value, and beyond a distance from the fuel surface of 0.3 mm the H_2O_2 is effectively completely consumed.

The decrease of $[H_2O_2]$ by reaction with Fe^{2+} can significantly reduce the fuel corrosion rate. This effect of Fe^{2+} also depends on the concentration of the other steel corrosion product, H_2. Fig. 4 shows the fuel corrosion rate (expressed as a flux of dissolved UO_2^{2+} away from the fuel surface) as a function of $[Fe^{2+}]_{bulk}$ in the presence of different $[H_2]_{bulk}$. In general, The UO_2^{2+} flux decreases rapidly as $[Fe^{2+}]$ increases from 0.01 to 0.1 μmol L^{-1}. For the highest $[H_2]_{bulk}$ (0.1 μmol L^{-1}), fuel corrosion is completely suppressed for $[Fe^{2+}]_{bulk} > 0.07$ μmol L^{-1}, while for a lower $[H_2]_{bulk}$ (0.01 μmol L^{-1}), complete suppression requires a bulk Fe^{2+} concentration of 1.5 μmol L^{-1}. It is noticed that, when $[Fe^{2+}]$ is greater than 4.2 μmol L^{-1} even the radiolytically produced H_2 can completely suppress fuel corrosion without any external H_2. This conclusion is in general agreement with the calculation of Jonsson et al. [37] considering the different fuel age (1000 vs. 100 years) and burnup (5–10 times lower for CANDU fuels compared to LWR fuels considered by Jonsson et al.).

In the previous model [38], calculations indicated that the corrosion rate was only reduced at an $[Fe^{2+}]$ of 1 μmol L^{-1} to ~ 60% of the value calculated ignoring any influence of Fe^{2+}. At the fuel surface the influence of Fe^{2+} is determined by the relative rates of H_2O_2 consumption by corrosion and the Fenton reaction, and the much greater sensitivity of the corrosion rate to $[Fe^{2+}]$ is primarily due to the changes in the model for UO_2 corrosion (Section 2.2). In this revised model the rate constant for H_2O_2-driven corrosion directly on the UO_2 surface (reaction (2a), Fig. 1) has been reduced by 3 orders of magnitude and the rate of reaction (2b) for corrosion catalyzed by H_2O_2 reduction on noble metal particles is greatly attenuated by the small percentage (1%) of particle coverage adopted. This significant reduction in overall fuel corrosion rate renders this rate much more sensitive to $[Fe^{2+}]$. Although relatively small by comparison, the incorporation of the full radiolysis reaction set also contributes to the enhanced effect.

3.3. Suppression of UO_2 corrosion by H_2

There are two possible mechanisms by which H_2 can suppress fuel corrosion: (i) it can suppress the radiolytic production of H_2O_2 by reactions in the radiolysis reaction set such as

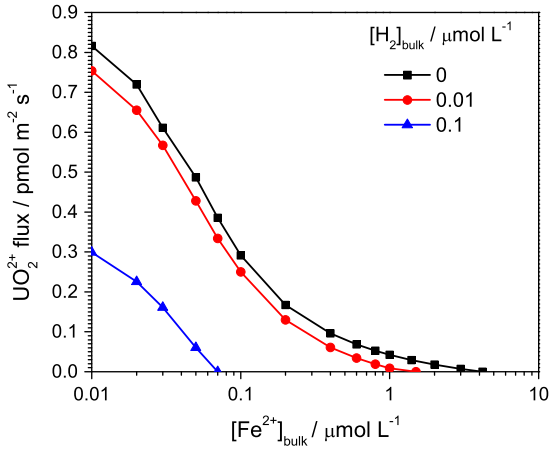

Fig. 4. The calculated diffusive flux of UO_2^{2+} (equivalent to UO_2 corrosion rate) as a function of bulk Fe^{2+} concentration; $[H_2]_{bulk}$ = 0, 0.01 and 0.1 μmol L^{-1}.

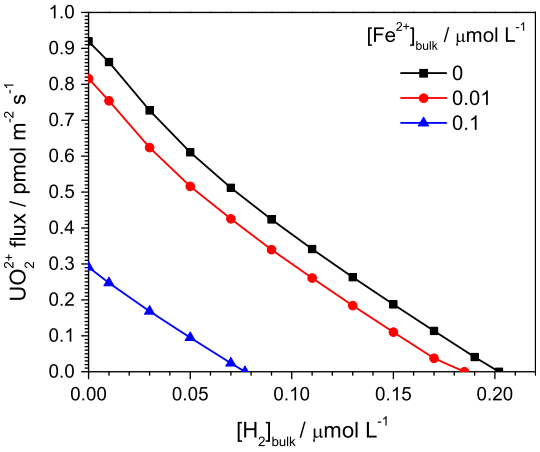

Fig. 6. The calculated diffusive flux of UO_2^{2+} (equivalent to UO_2 corrosion rate) as a function of bulk H_2 concentration; $[Fe^{2+}]_{bulk}$ = 0, 0.01 and 0.1 μmol L^{-1}.

$$OH^{\cdot} + H_2 \rightarrow H_2O + H^{\cdot} \quad (23)$$

$$H^{\cdot} + H_2O_2 \rightarrow H_2O + OH^{\cdot} \quad (24)$$

a chain reaction which becomes efficient when the $[H_2]$ is sufficiently high compared to the $[H_2O_2]$; (ii) H_2 can act as a reductant by catalytic reaction on noble metal particles (reaction (3a) in Fig. 1), and possibly also reverse the corrosion reaction via reactions (3b) and (3c) in Fig. 1 as described in Section 2.3.

Experimental studies showed that the presence of small concentrations of H_2 had only a minor effect on H_2O_2 production by α-radiolysis [73] and that any H_2 effect is strongly dependent on α dose rate and $[H_2]$ [74]. The calculations in Fig. 5 show the influence of H_2, at concentrations of 0.01–1 μmol L^{-1}, on the $[H_2O_2]$ profiles at two different $[Fe^{2+}]_{bulk}$. In contrast to the effect of the Fenton reaction (Fig. 3) the $[H_2O_2]$ is suppressed by <30% at these concentrations, consistent with the experimental expectations [73]. This demonstrates that the suppression of H_2O_2 production by H_2 is a relatively small contribution to the inhibiting effect of H_2 on fuel corrosion, consistent with the conclusions by Trummer et al. [74].

Fig. 6 shows the UO_2^{2+} flux (corrosion rate) is significantly suppressed as the bulk $[H_2]$ increases, which is consistent with the calculations in the previous model [38]. A close-to-linear decrease is obtained, and the UO_2 corrosion rate reaches zero for a specific $[H_2]_{bulk}$ (e.g. 0.202 μmol L^{-1} for $[Fe^{2+}]_{bulk}$ = 0) indicating that the rate of UO_2 oxidation/dissolution by H_2O_2 is balanced by the rate of its reduction by H_2. This concentration can be considered the critical H_2 concentration, $[H_2]_{crit}$, at which fuel corrosion is completely suppressed. The critical $[H_2]$ is about one order of magnitude less than that calculated previously [38]. This can be attributed partially to the new reaction scheme and rate constants adopted for UO_2 corrosion and also the use of a full reaction set for radiolysis. Trummer et al. [74] have also calculated the $[H_2]_{crit}$ required to prevent fuel corrosion for α-radiolysis in a closed system. For the same conditions ($D_R = 9.03 \times 10^5$ Gy a^{-1}, s_ε = 1%, and $[Fe^{2+}]$ = 0), they calculated $[H_2]_{crit}$ to be 0.0263 μmol L^{-1} comparing to our value of 0.202 μmol L^{-1}. One reason for this difference could be that our model is for an open system which connects with the surrounding groundwater environment, whereas that of Trummer et al. is for a closed system.

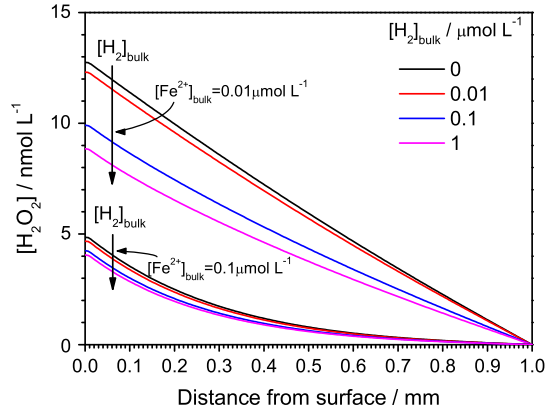

Fig. 5. Steady-state $[H_2O_2]$ profiles calculated for various bulk H_2 concentrations; $[Fe^{2+}]_{bulk}$ = 0.01 and 0.1 μmol L^{-1} as noted by arrows.

A second source of H_2 is radiolytic production. However, the calculated steady-state concentration of radiolytic H_2 at the fuel surface appears to be too low (<0.01 μmol L^{-1}, Fig. 2) to have a significant effect on UO_2 corrosion and its effect would be easily masked by the influence of external H_2 at a high $[H_2]_{bulk}$. A sensitivity test for the influence of radiolytic H_2 was performed for low $[H_2]_{bulk}$ (0 and 0.01 μmol L^{-1}). Removal of the radiolytic H_2 from the calculations leads to an increase in fuel corrosion rate by ~10% for both $[H_2]_{bulk}$ = 0 and 0.01 μmol L^{-1}.

Since the α-radiation fields associated with the fuel decay as the fuel ages, the $[H_2]$ requirement for complete suppression of fuel corrosion ($[H_2]_{crit}$) has been calculated as a function of decay time for a CANDU fuel bundle with a burnup of 220 MW h kg U^{-1}, Fig. 7. As expected, the $[H_2]_{crit}$ decreases markedly with time since emplacement in the repository. The increase in the H_2 requirement over the first 50 years reflects the accumulation of α-emitters as a consequence of the short-term γ/β decay of radionuclides within the fuel.

Fig. 7 also shows the influence of $[Fe^{2+}]_{bulk}$ on $[H_2]_{crit}$. The influence of Fe^{2+} is marked, the $[H_2]$ requirement dropping by an order of magnitude as $[Fe^{2+}]_{bulk}$ increases from 0 to 1 μmol L^{-1}. The trend is similar to that modelled by Jonsson et al. [37]. The higher $[H_2]_{crit}$ calculated by Jonsson et al. reflects the much higher burnup (about 5–10 times) of Swedish LWR fuel compared to CANDU fuel. This decrease in required $[H_2]_{crit}$ is consistent with experimental studies showing there is a threshold α-activity (corresponding to fuel within the age range 3000–55,000 years) below which no measurable effect of alpha radiolysis on fuel dissolution could be observed [15,75–77].

3.4. The influence of fuel burnup

By separating the reactions catalyzed on ε-particles from those on the UO_2 surface (as described in Section 2.2) it is possible to

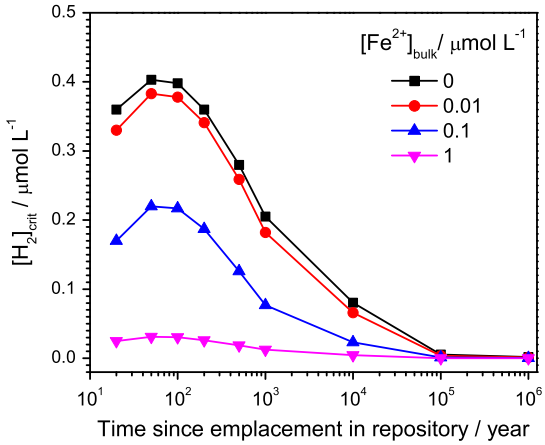

Fig. 7. The calculated $[H_2]_{crit}$ required to completely suppress fuel corrosion as a function of time since emplacement in repository at different $[Fe^{2+}]_{bulk}$.

attempt an estimate of the influence on corrosion of fuel burnup which determines the number density of ε-particles. Fig. 8 shows the corrosion rate as a function of ε-particle surface fraction (s_ε) for various $[H_2]_{bulk}$. As expected the effect of the surface fraction of ε-particles is very dependent on the $[H_2]_{bulk}$. For a low $[H_2]$ (0.1 μmol L^{-1}), the rate first increases until s_ε reaches 2.5% and then decreases. This reflects the balance between the catalytic effect of the ε-particles on both oxidation and reduction reactions, reaction (2b) and (3a) in Fig. 1. The maximum rate is achieved at an intermediate ε-particle surface fraction. When $[H_2]_{bulk}$ increases, the reduction reaction (3a) begins to dominate over the oxidation reaction (2b) leading to a decrease in corrosion rate with increasing s_ε. At $[H_2]_{bulk}$ = 0.15 μmol L^{-1}, an ε-particle fraction greater than 2.5% would result in complete suppression of fuel corrosion. As $[H_2]_{bulk}$ increases to 0.2 μmol L^{-1}, an even lower ε-particle fraction (i.e., fuel burnup) is required for effective inhibition of corrosion. This observation is consistent with experimental observations that a higher fraction of Pd (as surrogate ε-particles) results in a lower UO_2 dissolution rate [52] and that an increase in size and number density of ε-particles suppresses the corrosion potential on a series of SIMFUELs [26,53]. While the result for low $[H_2]_{bulk}$ is consistent with published observations that the highest fuel corrosion rates are achieved at intermediate burnups [78,79], caution should be exercised when making the comparison since the experiments were performed on spent fuel.

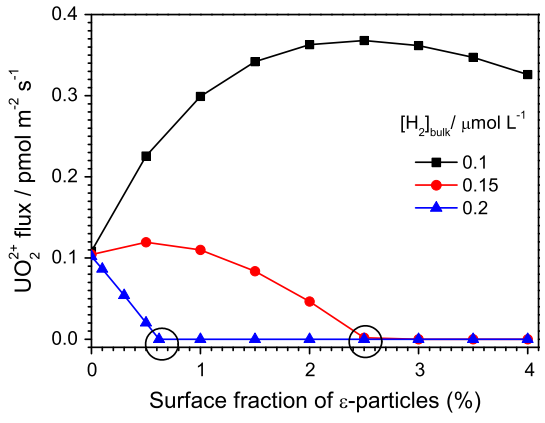

Fig. 8. The calculated diffusive flux of UO_2^{2+} (equivalent to UO_2 corrosion rate) as a function of ε-particle fraction for different bulk H_2 concentrations; $[Fe^{2+}]_{bulk}$ = 0.01 μmol L^{-1}.

4. Future model development

The current model represents a considerable improvement over our preliminary model since a more accurate reaction set is considered and recently published kinetic data is included.

One assumption in the current model is that the bulk concentrations of steel corrosion products will be constant. In reality, the supply of Fe^{2+} and H_2 will be determined by the corrosion performance of the steel vessel which will vary depending primarily on the available water. Consequently, the model could be improved by a more detailed analysis of the corrosion of the steel vessel. Presently, we are extending the model to 2-D/3-D to account for the effects of geometry on radiolytic corrosion occurring within fractured fuels, fuel grain boundaries, and fuel bundles. The local accumulation of radiolytic species and limited access to external H_2 and Fe^{2+} are expected to affect the fuel corrosion at these locations. Further model development to account for the influence of groundwater species such as chloride and carbonate on aqueous radiolysis and UO_2 corrosion is also required.

5. Conclusion

An improved model for nuclear fuel corrosion inside a failed waste container has been developed. A full α-radiolysis reaction set has been incorporated and the analysis shows that a simplified calculation which only accounts for the radiolytic production of H_2O_2/H_2 would provide a reasonable and conservative approximation, only overestimating H_2O_2 production and UO_2 corrosion rate by ~20%. Instead of assuming a single general reaction of H_2O_2 with the fuel surface, the direct reaction of UO_2 with H_2O_2 and the galvanically-coupled oxidation by H_2O_2 reduction on noble metal (ε) particles are both included. This allows the adoption of more experimentally justified rate constants and, by specifying the surface fraction of ε-particles, makes the model sensitive to fuel burnup. The surface-catalyzed decomposition of H_2O_2 appears to be the major pathway for H_2O_2 consumption on UO_2 and this effect has been included in this improved model.

The calculated fuel corrosion rate is very sensitive to $[Fe^{2+}]_{bulk}$ produced by corrosion of the steel vessel. When the $[Fe^{2+}]_{bulk}$ is greater than 4.2 μmol L^{-1} even the radiolytically produced H_2 alone can suppress fuel corrosion without assistance from external H_2 for CANDU fuel with an age of 1000 years or larger. The ability of H_2 to suppress fuel corrosion was shown to be sensitive to fuel burnup and able to completely suppress corrosion at bulk H_2 concentrations in the order of 0.1 μmol L^{-1}.

Acknowledgements

The authors thank Dr. Clara Wren and Dr. Jiju Joseph for discussions on water radiolysis. This research was funded under the Industrial Research Chair agreement between the Natural Science and Research Council (NSERC, Ottawa) and the Nuclear Waste Management Organization (NWMO, Toronto).

Reference

[1] L.H. Johnson, D.W. Shoesmith, Spent fuel, in: W. Lutze, R.C. Ewing (Eds.), Radioactive Waste Forms for the Future, Elsevier, Amsterdam, 1988.
[2] D.W. Shoesmith, Fuel corrosion waste process under waste disposal conditions, J. Nucl. Mater. 282 (2000) 1–31.
[3] B. Grambow, A. Loida, A. Martínex-Esparza, P. Díaz-Arocas, J. de Pablo, J.-L. Paul, J.-P. Glatz, K. Lemmens, K. Ollila, H. Christensen, Source Term for Performance Assessment of Spent Fuel as a Waste Form, Report EUR 19140 EN, European Commission, 2000.
[4] C. Poinssot, C. Ferry, M. Kelm, B. Grambow, A. Martinez Esparza Valiente, L.H. Johnson, Z. Andriambololona, J. Bruno, C. Cachoir, J.-M. Cavedon, H. Christensen, C. Corbel, C. Jegou, K. Lemmens, A. Loida, P. Lovera, F. Miserque, J. de Pablo, A. Poulesquen, J. Quinones, V. Rondinella, K. Spahiu, D.H. Wegen,

Final report of the European project spent fuel stability under repository conditions, Report CEA-R-6093, CEA, 2005.
[5] R.C. Ewing, and M.T. Peters, Source Term. In: OST&I Annual Report 2005, Report DOE/RW-0581, 2005, 5–51.
[6] F. Garisto, Fourth Case Study: Features, Events and Processes, Report TR-2012-14, Nuclear Waste Management Organization, Toronto, 2012.
[7] J. Bruno, R.C. Ewing, Spent nuclear fuel, Elements 2 (2006) 343–349.
[8] D.W. Shoesmith, Used Fuel and Uranium Dioxide Dissolution Studies - A Review, Report NWMO TR-2007-03, Nuclear Waste Management Organization, Toronto, ON, 2007.
[9] T.E. Eriksen, D.W. Shoesmith, M. Jonsson, Radiation induced dissolution of UO_2 based nuclear fuel – a critical review of predictive modelling approaches, J. Nucl. Mater. 420 (2012) 409–423.
[10] C.M. Lousada, M. Trummer, M. Jonsson, Reactivity of H_2O_2 towards different UO_2-based materials: the relative impact of radiolysis products revisited, J. Nucl. Mater. 434 (2013) 434–439.
[11] E. Ekeroth, O. Roth, M. Jonsson, The relative impact of radiolysis products in radiation induced oxidative dissolution of UO_2, J. Nucl. Mater. 355 (2006) 38–46.
[12] D.W. Shoesmith, The Role of Dissolved Hydrogen on the Corrosion/Dissolution of Spent Nuclear Fuel, Report NWMO TR-2008-19, Nuclear Waste Management Organization, Toronto, ON, 2008.
[13] SKB, Fuel and canister process report for the safety assessment SR-Site, Report TR-10-46, Swedish Nuclear Fuel and Waste Management Co. (SKB), Stockholm, 2010.
[14] K. Ollila, Y. Albinsson, V.M. Oversby, and M. Cowper, Dissolution rates of unirradiated UO_2, UO_2 doped with ^{233}U, and spent fuel under normal atmospheric conditions and under reducing conditions using an isotope dilution method, Report TR-03-13, Swedish Nuclear Fuel and Waste Management Co. (SKB), Stockholm, Sweden, 2003.
[15] K. Ollila, and V.M. Oversby, Dissolution of unirradiated UO_2 and O_2 doped with ^{233}U under reducing conditions, Report TR-05-07, Swedish Nuclear Fuel and Waste Management Co. (SKB), Stockholm, Sweden, 2005.
[16] K. Ollila, Dissolution of unirradiated UO_2 and UO_2 Doped with ^{233}U in 0.01 M NaCl under anoxic and reducing conditions, Report POSIVA 2006–08, Posiva Oy, Olkiluoto, Finland, 2006.
[17] Y. Albinsson, A. Ödegaard-Jensen, V.M. Oversby, L.O. Werme, Leaching of spent fuel under anaerobic and reducing conditions, in: R.J. Finch, D.B. Bullen (Eds.), Scientific basis for nuclear waste management XXVI, Materials Research Society. (Materials Research Society Symposium Proceedings 757), Warrendale, PA, 2003, p. 407–413.
[18] P. Carbol, P. Fors, S. Van Winckel, K. Spahiu, Corrosion of irradiated MOX fuel in presence of dissolved H_2, J. Nucl. Mater. 392 (2009) 45–54.
[19] K. Spahiu, L.O. Werme, U.B. Eklund, The influence of near field hydrogen on actinide solubilities and spent fuel leaching, Radiochim. Acta 88 (2000) 507–511.
[20] K. Spahiu, D. Cui, M. Lundström, The fate of radiolytic oxidants during spent fuel leaching in the presence of dissolved near field hydrogen, Radiochim. Acta 92 (2004) 625–629.
[21] S. Röllin, K. Spahiu, U.B. Eklund, Determination of dissolution rates of spent fuel in carbonate solutions under different redox conditions with a flow-through experiment, J. Nucl. Mater. 297 (2001) 231–243.
[22] E. Cera, J. Bruno, L. Duro, T.E. Eriksen, Experimental determination and chemical modelling of radiolytic processes at the spent fuel/water interface: long contact time experiments, Report TR-06-07, Swedish Nuclear Fuel and Waste Management Co. (SKB), Stockholm, Sweden, 2006.
[23] T.E. Eriksen, M. Jonsson, The effect of hydrogen on dissolution of spent fuel in 0.01 mol × dm^{-3} $NaHCO_3$ solution, Report TR-07-06, Swedish Nuclear Fuel and Waste Management Co. (SKB), Stockholm, Sweden, 2007.
[24] T.E. Eriksen, M. Jonsson, J. Merino, Modelling of time resolved and long contact time dissolution studies of spent nuclear fuel in 10 mM carbonate solution – a comparison between two different models and experimental data, J. Nucl. Mater. 375 (2008) 331–339.
[25] M.E. Broczkowski, J.J. Noël, D.W. Shoesmith, The inhibiting effects of hydrogen on the corrosion of uranium dioxide under nuclear waste disposal conditions, J. Nucl. Mater. 346 (2005) 16–23.
[26] M.E. Broczkowski, J.J. Noël, D.W. Shoesmith, The influence of dissolved hydrogen on the surface composition of doped uranium dioxide under aqueous corrosion conditions, J. Electroanal. Chem. 602 (2007) 8–16.
[27] M.E. Broczkowski, P.G. Keech, J.J. Noël, D.W. Shoesmith, Corrosion of uranium dioxide containing simulated fission products in dilute hydrogen peroxide and dissolved hydrogen, J. Electrochem. Soc. 157 (2010) C275–C281.
[28] E. Ekeroth, M. Jonsson, T.E. Eriksen, K. Ljungqvist, S. Kovacs, I. Puigdomenech, Reduction of UO_2^{2+} by H_2, J. Nucl. Mater. 334 (2004) 35–39.
[29] M. Trummer, S. Nilsson, M. Jonsson, On the effects of fission product noble metal inclusions on the kinetics of radiation induced dissolution of spent nuclear fuel, J. Nucl. Mater. 378 (2008) 55–59.
[30] S. Nilsson, M. Jonsson, On the catalytic effects of UO_2(s) and Pd(s) on the reaction between H_2O_2 and H_2 in aqueous solution, J. Nucl. Mater. 372 (2008) 160–163.
[31] S. Nilsson, M. Jonsson, On the catalytic effects of Pd(s) on the reduction of UO_2^{2+} with H_2 in aqueous solution, J. Nucl. Mater. 374 (2008) 290–292.
[32] H. Christensen, S. Sunder, D.W. Shoesmith, Oxidation of nuclear fuel (UO_2) by the products of water radiolysis, development of a kinetic model, J. Alloys Compd. 213 (214) (1994) 93–99.
[33] H. Christensen, Calculations simulating spent-fuel leaching experiments, Nucl. Technol. 124 (1998) 165–174.
[34] A. Poulesquen, C. Jegou, Influence of Alpha radiolysis of water on UO_2 matrix alteration: chemical/transport model, Nucl. Technol. 160 (2007) 337–345.
[35] D.W. Shoesmith, M. Kolar, F. King, A mixed-potential model to predict fuel (uranium dioxide) corrosion within a failed nuclear waste container, Corrosion 59 (9) (2003) 802–816.
[36] M. Kolar, F. King, Report No. 06819-REP-01200-10104-R00, Ontario Power Generation, 2003.
[37] M. Jonsson, F. Nielsen, O. Roth, E. Ekeroth, S. Nilsson, M.M. Hossain, Radiation induced spent nuclear fuel dissolution under deep repository conditions, Environ. Sci. Technol. 41 (20) (2007) 7087–7093.
[38] L. Wu, Y. Beauregard, Z. Qin, S. Rohani, D.W. Shoesmith, A model for the influence of steel corrosion products on nuclear fuel corrosion under permanent disposal conditions, Corros. Sci. 61 (2012) 83–91.
[39] R. Pehrman, M. Trummer, C.M. Lousada, M. Jonsson, On the redox reactivity of doped UO_2 pellets – influence of dopants on the H_2O_2 decomposition mechanism, J. Nucl. Mater. 430 (2012) 6–11.
[40] D.W. Shoesmith, The chemistry/electrochemistry of spent nuclear fuel as a wasteform, in: P. Burns, G. Sigmon (Eds.), Uranium: Cradle to Grave, Mineralogical Society of Canada, Short Course Series, vol 43, 2013, pp. 337–368 (and references therein).
[41] F. Garisto, D.H. Barber, E. Chen, A. Inglot, C.A. Morrison, Alpha, Beta and Gamma Dose Rates in Water in Contact with Used CANDU Fuel, Report NWMO TR-2009-27, Nuclear Waste Management Organization, Toronto, ON, 2009.
[42] F. Nielsen, M. Jonsson, Geometrical α- and β-dose distributions and production rates of radiolysis products in water in contact with spent nuclear fuel, J. Nucl. Mater. 359 (2006) 1–7.
[43] A. Poulesquen, C. Jégou, S. Peuget, Determination of alpha dose rate profile at the UO_2/water interface, in: P. Van Iseghem (Ed.), Scientific basis for nuclear waste management XXIX, Material Research Society (Mater. Res. Soc. Symp. Proc. 932), Warrendale, PA, 2006, pp. 505–512.
[44] S. Sunder, Calculation of radiation dose rates in a water layer in contact with used CANDU UO_2 fuel, Nucl. Technol. 122 (1998) 211–221.
[45] J.W.T. Spinks, R.J. Woods, An Introduction to Radiation Chemistry, third ed., John Wiley & Sons Inc., New York, 1990.
[46] F. Garisto, J. Avis, N. Calder, A. D'Adrea, P. Gierszewski, C. Kitson, T. Melnyk, K. Wei, L. Wojciechowski, Third case study – defective container scenario, Report 06219-REP-01200-10126-R00, Ontario Power Generation, Toronto, ON, 2004.
[47] G. Choppin, J.O. Liljenzin, J. Rydberg, Radiochemistry and Nuclear Chemistry, Butterworth-Heinemann, Oxford, 2001.
[48] J.S. Goldik, J.J. Noël, D.W. Shoesmith, The electrochemical reduction of hydrogen peroxide on uranium dioxide electrodes in alkaline solution, J. Electroanal. Chem. 582 (2005) 241–248.
[49] J.S. Goldik, J.J. Noël, D.W. Shoesmith, The effects of simulated fission products in the reduction of hydrogen peroxide on simulated nuclear fuel electrodes, J. Electrochem. Soc. 153 (2006) E151–E159.
[50] F. Nielsen, M. Jonsson, Simulations of H_2O_2 concentration profiles in the water surrounding spent nuclear fuel taking mixed radiation fields and bulk reactions into account, J. Nucl. Mater. 374 (2008) 281–285.
[51] S. Nilsson, M. Jonsson, H_2O_2 and radiation induced dissolution of UO_2 and SIMFUEL pellets, J. Nucl. Mater. 410 (2011) 89–93.
[52] M. Trummer, O. Roth, M. Jonsson, H_2 inhibition of radiation induced dissolution of spent nuclear fuel, J. Nucl. Mater. 383 (2009) 226–230.
[53] M.E. Broczkowski, D. Zagidulin, D.W. Shoesmith, The role of dissolved hydrogen on the corrosion/dissolution of spent nuclear fuel, in: "Nuclear Energy and the Environment", American Chemical Society Symposium, 2010, vol. 1046, Chapter 26, pp. 349–380.
[54] P. Carbol, J. Cobos-Sabate, J.-P. Glatz, C. Ronchi, V. Rondinella, D.H. Wegen, T. Wiss, A. Loida, V. Metz, B. Kienzler, K. Spahiu, B. Grambow, J. Quinones, A. Martinez Esparza Valiente, The effect of dissolved hydrogen on the dissolution of ^{233}U-doped UO_2(s), high burn-up spent fuel and MOX fuel, Report TR-05-09, Swedish Nuclear Fuel and Waste Management Company, 2005.
[55] F.J. Millero, S. Sotolongo, The oxidation of Fe(II) with H_2O_2 in seawater, Geochim. Cosmochim. Acta 53 (1989) 1867–1873.
[56] F. Garisto, T. Kempe, P. Gierszewski, Technical summary of the saftey aspects of the deep geological repository concept for used nuclear fuel, Report NWMO TR-2009-12, Nuclear Waste Management Organization, Toronto, ON, 2009.
[57] D.G. Bennett, R. Gens, Overview of European concepts for high-level waste and spent fuel disposal with special reference waste container corrosion, J. Nucl. Mater. 379 (2008) 1–8.
[58] J. Kaija, K. Rasilainen, R. Blomqvist, The use of selected safety indicators (concentrations, fluxes) in the assessment of radioactive waste disposal – Report 6, Report YST-114, Geological Survey of Finland – Nuclear Waste Disposal Research, 2003.
[59] W. Xu, K. Daub, X. Zhang, J.J. Noël, D.W. Shoesmith, J.C. Wren, Oxide formation and conversion on carbon steel in mildly basic solutions, Electrochim. Acta 54 (2009) 5727–5738.
[60] C.C. Lin, F.R. Smith, N. Ichikawa, T. Baba, M. Itow, Decomposition of hydrogen peroxide at elevated temperatures, Int. J. Chem. Kinet. 23 (1991) 971–987.
[61] A. Hiroki, J.A. LaVerne, Decomposition of hydrogen peroxide at water-ceramic oxide interface, J. Phys. Chem. B 109 (2005) 3364–3370.
[62] A.J. Elliot, D.M. Bartels, The reaction set, rate constants and g-values for the simulation of the radiolysis of light water over the range 20 to 350 °C Based on

Information Available in 2008, Report 153-127160-450-001, AECL, Mississauga, ON, 2009.
[63] J.C. Wren, D.W. Shoesmith, S. Sunder, Corrosion behavior of uranium dioxide in alpha radiolytically decomposed water, J. Electrochem. Soc. 152 (2005) B470.
[64] C.M. Lousada, M. Jonsson, Kinetics, mechanism, and activation energy of H_2O_2 decomposition on the surface of ZrO_2, J. Phys. Chem. C 114 (2010) 11202–11208.
[65] C.M. Lousada, A.J. Johansson, T. Brinck, M. Jonsson, Mechanism of H_2O_2 decomposition on transition metal oxide surfaces, J. Phys. Chem. C 116 (2012) 9533–9543.
[66] M. Razdan, D.W. Shoesmith, Influence of trivalent-dopants on the structural and electrochemical properties of uranium dioxide (UO_2), J. Electrochem. Soc. 161 (2014) H105–H113.
[67] F.R. Duke, T.W. Haas, The homogeneous base-catalyzed decomposition of hydrogen peroxide, J. Phys. Chem. 65 (1961) 304–306.
[68] H.M. Cota, T. Katan, M. Chin, F.J. Schoenweis, Decomposition of dilute hydrogen peroxide in alkaline solutions, Nature 203 (1964) 1281.
[69] C. Walling, R.E. Partch, T. Weil, Kinetics of the decomposition of hydrogen peroxide catalyzed by ferric ethylenediaminetetraacetate complex, Proc. Natl. Acad. Sci. 72 (1975) 140–142.
[70] O. Spalek, J. Balej, I. Paseka, Kinetics of the decomposition of hydrogen peroxide in alkaline solutions, J. Chem. Soc., Faraday Trans. 1 (78) (1982) 2349–2359.
[71] J.F. Perez-Benito, Iron(III)-hydrogen peroxide reaction: kinetic evidence of a hydroxyl-mediated chain mechanism, J. Phys. Chem. A 108 (2004) 4853–4858.
[72] C. Corbel, G. Sattonnay, S. Guilbert, F. Garrido, M.F. Barthe, C. Jegou, Addition versus radiolytic production effects of hydrogen peroxide on aqueous corrosion of UO_2, J. Nucl. Mater. 348 (2006) 1–17.
[73] B. Pastina, J.A. LaVerne, Effect of molecular hydrogen on hydrogen peroxide in water radiolysis, J. Phys. Chem. A 105 (2001) 9316–9322.
[74] M. Trummer, M. Jonsson, Resolving the H_2 effect on radiation induced dissolution of UO_2-based spent nuclear fuel, J. Nucl. Mater. 396 (2010) 163–169.
[75] V. Rondinella, J. Cobos, T. Wiss, Leaching behaviour of low-activity alpha-doped UO_2, in: J.M. Hanchar, S. Stroes-Gascoyne, L. Browning (Eds.), Scientific Basis for Nuclear Waste Management XXVIII, Materials Research Society, Warrendale, PA, 2004, pp. 167–173.
[76] B. Muzeau, C. Jégou, F. Delaunay, V. Broudic, A. Brevet, H. Catalette, E. Simoni, C. Corbel, Radiolytic oxidation of UO_2 pellets doped with alpha emitters (^{238}/^{239}Pu), J. Alloys Compd. 467 (2009) 578–589.
[77] C. Poinssot, C. Ferry, A. Poulesquen, New perspectives for the spent nuclear fuel radionuclides release model in a deep geological repository, in: D. Dunn, C. Poinssot, B. Begg (Eds.), Scientific Basis for Nuclear Waste Management XXX, Materials Research Society, Warrendale, PA, 2007, pp. 111–116.
[78] E. Ekeroth, J. Low, H.-U. Zwicky, K. Spahiu, Corrosion studies with high burnup LWR fuel in simulated groundwater, in: N.C. Hyatt, D.A. Pickett, R.B. Rebak (Eds.), Scientific Basis for Nuclear Waste Management XXXII, Materials Research Society, Warrendale, PA, 2009, pp. Q02–Q07.
[79] C. Jegou, S. Peuget, V. Broudic, D. Roudil, X. Deschanels, J.M. Bart, Identification of the mechanism limiting the alteration of clad spent fuel segments in aerated carbonated groundwater, J. Nucl. Mater. 326 (2004) 144–155.
[80] J. Joseph, B. Seonchoi, P. Yakabuskie, J.C. Wren, A combined experimental and model analysis on the effect of pH and O_2(aq) on γ-radiolytically produced H_2 and H_2O_2, Radiat. Phys. Chem. 77 (2008) 1009–1020.